Bulgarian Chemical Communications, Volume 52, Issue 3 (pp. 342-347) 2020 DOI: 10.34049/bcc.52.3.5134

CO_2 methanation over Co–Ni/Al_2O_3 and Co–Ni/SiC catalysts

A. G. Dyachenko[1], O. V. Ischenko[1], M. G. Zhludenko[2], S. V. Gaidai[1],
T. M. Zakharova[1], A. V. Yatsymyrskyi[1], V. V. Lisnyak[1*]

[1] *Chemical Faculty, Taras Shevchenko National University of Kyiv, 64, Volodymyrska Str., 01033 Kyiv, Ukraine*
[2] *Ukrorgsyntez Ltd, 67, Chervonotkatska Str., 02002 Kyiv, Ukraine*

Received: April 15, 2019; Revised: March 23, 2020

In this study, highly loaded 20 wt% (Co_xNi_{100-x})/Al_2O_3 and (Co_xNi_{100-x})/SiC catalysts, where x = 0, 20, 60, 80, and 100 wt%, were prepared by a three-stage method, which includes wet impregnation of Al_2O_3 and SiC with the metal nitrates, thermal decomposition of the loaded nitrates, and obtaining of the loaded metals by reducing their oxides with hydrogen at 350 °C. The prepared catalysts were examined by different methods and tested in the CO_2 methanation. Scanning electron microscopy and X-ray powder diffraction studies showed a difference in the loaded particle dispersion and the phase composition of catalysts. The highly loaded 20 wt% Co–Ni/Al_2O_3 catalysts showed the highest catalytic activity. In the presence of 20 wt% $Co_{60}Ni_{40}/Al_2O_3$, 20 wt% $Co_{80}Ni_{20}/Al_2O_3$, and 20 wt% Co_{100}/Al_2O_3 catalysts, 100% CO_2 can be converted into CH_4 at 300 °C. This temperature is lower by 100 °C than the temperature at the total conversion over 20 wt% (Co–Ni)/SiC catalysts. Thermal desorption mass spectroscopy revealed that the methanation of CO_2 passed through the formation of CHO* intermediate over the most active 20 wt% $Co_{80}Ni_{20}/Al_2O_3$ and 20 wt% $Co_{80}Ni_{20}$/SiC catalysts.

Keywords: Carbon dioxide methanation, Renewable fuels, Highly loaded Co–Ni catalysts, Alumina, Carborundum.

INTRODUCTION

Modern levels of energy consumption require identifying, preparing, and using new energy resources. Despite the growing role of renewable energy sources, organic fossil fuels remain the basic resources of energy. Their use has increased the amount of anthropogenic carbon dioxide (CO_2) and carbon monoxide (CO) in the atmosphere [1–3]. The average increase in CO_2 emissions *per annum* is about 2.2%. In this situation, an attractive problem solution is converting CO_2 into an eco-fuel, creating methane gas. By capturing CO_2 from the atmosphere and generating methane, we could solve environmental and energy problems. For the methanation reaction, the most used catalysts are based on nickel and cobalt metals [2–5]. Today, alumina (Al_2O_3) and carborundum (SiC) are valuable carriers/components that provide thermo-mechanical resistance for catalysts [6, 7]. The potential of catalysts, which were prepared by combining bimetallic active phase and inert carriers, was partially explored and reported in [8, 9].

In the present study, we reported on the activity and selectivity of Co–Ni/Al_2O_3 and Co–Ni/SiC catalysts in the CO_2 methanation. To find correlations between the catalyst activity and other physicochemical characteristics, we examined them by scanning electron microscopy (SEM), X-ray powder diffraction (XRPD), and thermal desorption mass spectroscopy (TD MS).

EXPERIMENTAL

Materials

Reakhim Al_2O_3 and SiC powders were products of reagent quality. The metal nitrate salts, nickel nitrate hexahydrate ($Ni(NO_3)_2 \cdot 6H_2O$) and cobalt nitrate hexahydrate ($Co(NO_3)_2 \cdot 6H_2O$), were purchased from Aldrich.

Preparation

Both Al_2O_3 and SiC carriers were wet impregnated with the required quantity of $Co(NO_3)_2$ and $Ni(NO_3)_2$ aqueous solutions prepared from the respective hexahydrates. The metal salt solutions contained, according to the desired Ni and/or Co loading, different masses of dissolved $Ni(NO_3)_2$ or/and $Co(NO_3)_2$, which were accounted in such a way, to prepare 20 wt% (Co_xNi_{100-x})/Al_2O_3 and 20 wt% (Co_xNi_{100-x})/(SiC) catalysts, where x = 0, 20, 60, 80, and 100 wt%.

During wet impregnation, the selected carrier (Al_2O_3 or SiC) was placed in a glass beaker, and aqueous solutions of $Ni(NO_3)_2$ or $Co(NO_3)_2$, or their mixed solution with a volume significantly higher than the pore volume of the carrier was added. The water from the solutions impregnating the carrier solids was vaporized on a thermostat bath at 80 °C in an evaporating dish, and afterward, the resulting solid samples were air-dried for 12

---

* To whom all correspondence should be sent:
E-mail: lisnyak@chem.univ.kiev.ua

hours at 120 °C.

The prepared samples containing cobalt and nickel oxides were reduced in a quartz glass reactor at atmospheric pressure. For the reduction, 0.5 cm of quartz wool and 2.0 g of the dried solid were packed in the reactor, and a thermocouple was placed directly within the packed bed. Hydrogen gas, which was used for reduction, was diluted with helium up to 50 vol% helium concentration in the resulting H_2–He mixture. The reduction in flowing hydrogen (volumetric flow: 100 mL/min) occurred at 350 °C within 120 min (heating rate: 10 °C/min). As a result, an active phase, in the form of bimetallic Co/Ni particles, was formed on the surface of the carriers.

Catalytic test

The methanation of CO_2, according to the reaction $CO_2 + H_2 = CH_4 + H_2O$, was carried out in the presence of a catalyst in a fixed-bed quartz reactor at atmospheric pressure. The catalyst packed volume and the catalyst mass were 1 cm^3 and 1 g, correspondingly, and the major portion of particles was between 40 and 100 mesh. The closed packed reactor was placed in a programmable resistive furnace, and then the catalysts sample was treated in the reaction mixture under gradually raised temperature from 30 to 450 °C (heating rate: 10 °C/min). The reaction temperature inside the catalyst layer was monitored with a covered thermopile. A thermal conductivity detector on a Shimadzu GC 2014 gas chromatograph was used to analyze the outlet and inlet gas mixtures. All gases were separated for the analysis on a 1.0 m chromatographic column packed with molecular sieves. For the catalytic CO_2 methanation [10, 11], the conversion of CO_2 (X_{CO2}) and the yields of CO and CH_4 (Y_{CO} and Y_{CH4}) were calculated from the equations:

$$X_{CO_2}(\%) = \frac{[CO_2]_{in} - [CO_2]_{out}}{[CO_2]_{in}} \times 100 \qquad (1)$$

$$Y_{CO}(\%) = \frac{[CO]_{out}}{[CO_2]_{in}} \times 100 \qquad (2)$$

$$Y_{CH_4}(\%) = \frac{[CH_4]_{out}}{[CO_2]_{in}} \times 100 \qquad (3)$$

where $[CO_2]_{in}$, $[CO_2]_{out}$, $[CO]_{out}$, and $[CH_4]_{out}$ are the gas volume concentrations in mixtures sampled at the inlet and outlet (see respective indices) of the catalytic reactor.

Characterization

Morphological studies and microanalysis were carried out on a MIRA3 Tescan scanning electron microscope equipped with an energy-dispersive X-ray spectroscopy analyzer (EDX) for elemental analysis.

XRPD patterns were collected on a Dron-4-07 diffractometer; the wavelength of CuKα radiation was used. Phase analysis was performed using structural data available in open crystallographic databases or can be extracted for single phases from open databases for powder diffraction. Specific surface areas (S_{sp}) were measured by argon adsorption at –196.15 °C and 25 °C.

The catalyst samples for the TD MS studies were prepared in the same reactor and under the same conditions used for the catalytic tests. Upon reaching the temperature at a maximum CO_2 conversion, the methanation in the presence of a selected catalyst was carried out for 2 hours at the stated temperature, and then the catalytic reactor was quenched to room temperature under the flow of the reaction mixture. Afterward, the sampled mass was transferred under the flow of reacting gases to a quartz glass ampoule, and then the ampule was vacuumed. All operations were carried out at room temperature using standard Schlenk techniques. Under the stated conditions of the catalyst sampling, we fixed the surface of the catalyst covered with adsorbed products, reagents, and intermediate compounds. Subsequently, we collected structural information on the adsorbed particles, including those involved in the CO_2 methanation reaction, directly from the fragmentation pattern of molecules which was registered by the electron impact ionization mass spectroscopy (MS) method.

For this purpose, after vacuum sealing, the ampoule with the sample was disconnected from the vacuum pump, and the ampule's outlet was connected online to the ionization source of a unipolar quadruple mass-spectrometer (Selmi, MX7304A model). MS data were acquired from the m/z range 10–100, and thermal desorption (TD) profiles were registered in the temperature range from ambient temperature to 800 °C, under the heating rate of 14 °C/min [12]. The constant heating rate was provided by a toroidal (elliptical) electric heater concentrating heat onto the ampoule. The temperature was controlled with a type K thermocouple positioned in the thermowell of the ampoule. This thermocouple was placed as close as possible to the catalyst sample. The working vacuum was varied from 10^{-4} to 10^{-5} Pa that allowed the detection of very small amounts of desorbed particles ($10^{–4}$ to $10^{–5}$ moles/m^3). Considering the TD profiles and the current of desorbed particles registered in the positive ion mode, one can qualitatively characterize the processes occurring on the surface of the catalyst, and one can propose the possible mechanism of the reaction.

RESULTS AND DISCUSSION

According to Table 1, the prepared monometallic and bimetallic catalysts highly loaded onto the Al_2O_3 exhibit from 96% to 100% selectivity in the methanation reaction at 250 °C and above. In general, the reaction selectivity increases with increasing the reaction temperature, decreasing the yield of CO to 0%. Under the optimized reaction conditions, 71% and 100% CO_2 conversion and nearly 100% CH_4 selectivity were achieved over 20 wt% Ni_{100}/Al_2O_3 and 20 wt% Co_{100}/Al_2O_3 catalysts, correspondingly, with good stability at 350 °C for over 24 h. An increase in the amount of Co (from 20 to 80 wt%) in the bimetallic 20 wt% $Co_xNi_{100–x}/Al_2O_3$ catalysts leads to an increase in the yield of methane (Table 1). Our findings show the 100% CO_2 conversion to CH_4 in the presence of 20 wt% $Co_{60}Ni_{40}/Al_2O_3$ and 20 wt% $Co_{80}Ni_{20}/Al_2O_3$ catalysts at the lowest reaction temperature of 300 °C.

Al_2O_3 and SiC have different physicochemical characteristics, such as S_{sp}, temperature stability, and affinity to metal or metal oxide. The catalysts of 20 wt% Co–Ni/SiC series are operated at higher reaction temperatures (Table 2). The tendency to increase the yield of CH_4 stays the same at increasing the reaction temperature and the Co content in the bimetal 20 wt% $Co_xNi_{100–x}$/SiC catalysts.

Table 1. Parameters for the catalysts of 20 wt% Co–Ni/Al_2O_3 series.

Catalyst	**$^aS_{sp}$ (m^2/g)**	**Reaction temperature (°C)**			
		200	250	300	350
		^{b}Yield, Y_{CH_4}/Y_{CO} (%)			
20 wt% Ni_{100}/Al_2O_3	68	2/2	60/2	68/2	69/2
20 wt% $Co_{20}Ni_{80}/Al_2O_3$	65	5/2	44/2	70/1	83/1
20 wt% $Co_{60}Ni_{40}/Al_2O_3$	62	11/2	61/1	100/0	100/0
20 wt% $Co_{80}Ni_{20}/Al_2O_3$	58	14/1	69/1	100/0	100/0
20 wt% Co_{100}/Al_2O_3	52	6/1	58/2	83/0	100/0

$^aS_{sp}$ (Al_2O_3) = 68 m^2/g. ^{b}Conversion of CO_2 = $Y_{CH_4} + Y_{CO}$.

Table 2. Parameters for the catalysts of 20 wt% Co–Ni/SiC series.

Catalyst	**$^aS_{sp}$ (m^2/g)**	**Reaction temperature (°C)**			
		300	350	400	450
		^{b}Yield, Y_{CH_4}/Y_{CO} (%)			
20 wt% Ni_{100}/SiC	0.6	0.5/6	4/21	22/29	36/30
20 wt% $Co_{20}Ni_{80}$/SiC	1.0	3/9	16/23	66/5	80/1
20 wt% $Co_{40}Ni_{60}$/SiC	0.5	3/8	13/20	51/3	86/1
20 wt% $Co_{60}Ni_{40}$/SiC	1.0	15/9	81/3	98/1	100/0
20 wt% $Co_{80}Ni_{20}$/SiC	2.0	89/1	96/0	98/0	100/0
20 wt% Co_{100}/SiC	2.0	68/1	82/1	86/1	98/1

$^aS_{sp}$ (SiC) = 0.6 m^2/g. ^{b}Conversion of CO_2 = $Y_{CH_4} + Y_{CO}$.

Approximately 100% CO_2 conversion to CH_4 was achieved on 20 wt% Co_{100}/SiC, 20 wt% $Co_{60}Ni_{40}$/SiC, and 20 wt% $Co_{80}Ni_{20}$/SiC catalysts at 450 °C. According to Table 2, 20 wt% Ni_{100}/SiC, 20 wt% $Co_{20}Ni_{80}$/SiC, and 20 wt% $Co_{40}Ni_{60}$/SiC catalysts showed 25–40% selectivity towards CH_4 at 300–350 °C. For 20 wt% Ni_{100}/SiC, 20 wt% $Co_{20}Ni_{80}$/SiC, and 20 wt% $Co_{40}Ni_{60}$/SiC catalysts, Y_{CO} depends on the reaction temperature and can reach about 20% at 350 °C. Considering available temperature dependencies, we suggest that the dissociation of CO_2 is the methanation limiting step for all studied catalysts. That is why the yield of CH_4 shows a significant increase with increasing temperature, simultaneously reducing the yield of CO. Considering the results of the catalytic test, we suggest that the ratio of Co (60–80%) to Ni (40–20%) in the active complex of catalysts has a positive influence on the performance and promotes the course of surface methanation, regardless of the used carrier. Below, we will point on the main differences in the TD profiles on an example of 20 wt% $Co_{80}Ni_{20}/Al_2O_3$ and 20 wt% $Co_{40}Ni_{60}$/SiC catalysts that have higher and lower catalytic activity, correspondingly. Figure 1a shows the typical temperature profiles of particles found after catalysis over high-activity catalysts ($Y_{CH4} \approx 100\%$ at above 300 °C). Up to 100 °C, we registered intensive desorption of the adsorbed H_2O (m/z 18), CO_2 (m/z 44), and CO (m/z 28). According to Karelovic and Ruiz [13], multiple ways to methanation are known nowadays. Among them, the mechanism presented below is in good agreement with the TD MS data.

$$CO_2 \rightarrow CO_{2,\,ads} \quad (4)$$

$$CO_{2,\,ads} \rightarrow CO_{ads} + O_{ads} \quad (5)$$

$$H_{2,\,ads} \rightarrow 2H_{ads} \quad (6)$$

$$CO_{ads} + H_{ads} \rightarrow CHO_{ads} \quad (7)$$

$$CHO_{ads} + H_{ads} \rightarrow CH_2O_{ads} \quad (8)$$

$$CH_2O_{ads} + 2H_{ads} \rightarrow CH_{3,\,ads} + OH_{ads} \quad (9)$$

$$CH_{3,\,ads} + H_{ads} \rightarrow CH_{4,\,ads} \quad (10)$$

$$OH_{ads} + H_{ads} \rightarrow H_2O \quad (11)$$

As can be seen in Fig. 1a, CO_2, CO, CH_4, CH_3*, and COH* are released simultaneously between 400 and 550 °C. Their thermal desorption peaks are seen at ~450 °C. In our opinion, the dissociation of CO_2 molecules (CO + O) and the formation of CH_4 molecules, as the target product, through intermediates (CH_3* and COH*) [14], take place simultaneously in this temperature range. Therefore, we can assume that the CO_2 methanation reaction over high-activity 20 wt% Co–Ni/Al_2O_3 catalysts proceeds by the substitution of oxygen atoms in CO for hydrogen atoms.

Figure 1b presents the TD profiles of desorbed particles registered after catalysis over the 20 wt% $Co_{40}Ni_{60}$/SiC catalyst that showed lower activity at medium-temperature CO_2 methanation ($Y_{CH4} \leq 70\%$ at 300–400 °C). In contrast to the TD profiles of high-activity catalysts, the profile of CO_2 has peaked at 120, 360, and 540 °C. The peaks do not necessarily coincide with thermal desorption peaks of CO and COH*. This is because of the surface coverage with adsorbed CO molecules. As follows from the presented profiles, dissociating CO_2 molecules have saturated the surface layer with CO. Adsorbed CO gradually interacts with adsorbed hydrogen and blocks the surface of loaded metals, slowing down the overall methanation rate [15, 16].

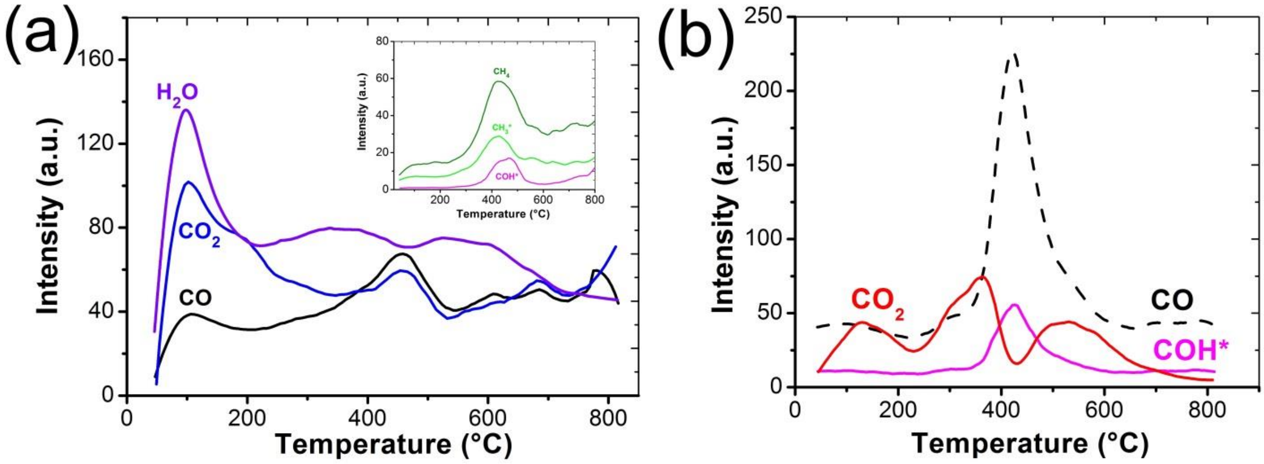

Figure 1. TD profiles of particles adsorbed on (a) 20 wt% $Co_{80}Ni_{20}/Al_2O_3$ and (b) 20 wt% $Co_{40}Ni_{60}$/SiC catalysts.

Below, we will consider SEM and XRPD data for the typical representatives of the catalyst series. SEM images of 20 wt% $Co_{80}Ni_{20}/Al_2O_3$ after catalysis have shown that the agglomerated particles ranged from 10 to 100 microns (Figure 2a).

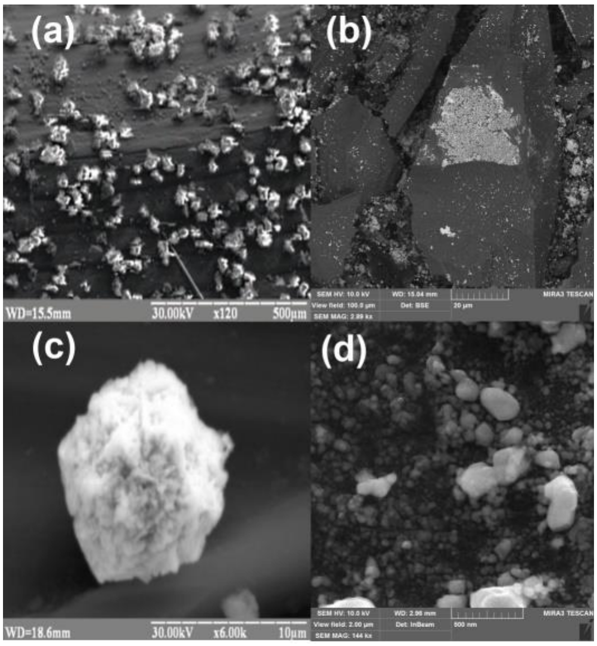

Figure 2. SEM micrographs of (a, c) 20 wt% $Co_{80}Ni_{20}/Al_2O_3$ and (b, d) 20 wt% $Co_{80}Ni_{20}$/SiC catalysts, (c, d) micrographs of higher magnification.

Their average size is about 30 microns, and the particles have many grains showing a rough structure of the surface and many cavities. The microanalysis data for 20 wt% $Co_{80}Ni_{20}/Al_2O_3$ catalyst (53.7 mass% Al, 19.7 mass% O, 20.7 mass% Co and 5.9 mass% Ni) showed that 30% of the active mass is uniformly present on the surface. The ratio between cobalt and nickel is 78:22, which is practically the same as was calculated. The uniform distribution of the particles of the active mass on the alumina surface has a positive effect on the catalytic activity of 20 wt% Co–Ni/Al_2O_3 in the CO_2 methanation reaction. The wet impregnation used here cannot provide uniform loading of the metal masses on the surface of Al_2O_3. Therefore, the EDX analysis of the $Co_{80}Ni_{20}/Al_2O_3$ sample shows the surface area with the overstated amount of the loaded Co and Ni metals of 30 wt%.

For the smooth SiC surface (Fig. 2b), the loaded Co and Ni masses are unevenly distributed (the load was varied from 30 to 90 wt%). Particles of size from 50 nm to large agglomerates up to 20 μm are observed. The large agglomerates are composed of volumetric porous particles of 20–300 nm in size. In contrast to the 20 wt% Co–Ni/Al_2O_3 catalysts, the specific surface area of 20 wt% Co–Ni/SiC catalysts is small (Table 2). Figure 3 presents typical XRPD patterns of higher activity catalysts, on the example of $Co_{80}Ni_{20}/Al_2O_3$ catalyst, and lower activity catalysts, on the example of $Co_{80}Ni_{20}$/SiC catalyst, studied after the catalytic experiments. Room temperature XRPD patterns were collected for the samples of $Co_{80}Ni_{20}/Al_2O_3$ and $Co_{80}Ni_{20}$/SiC catalysts that had worked 10 hours or more in the reaction medium at 300 °C and 450 °C, respectively.

After catalysis, the crystalline phases of corundum Al_2O_3, boehmite γ-AlO(OH), and γ-Al_2O_3 were found in the composition of 20 wt% $Co_{80}Ni_{20}/Al_2O_3$ and 20 wt% $Co_{60}Ni_{40}/Al_2O_3$ catalysts. We also registered cobalt oxide (Co_3O_4), hexagonal close-packed phases of Ni and Co metals, and, possibly, of Ni–Co alloys with partial substitution of Co for Ni. Broad reflexes of the Co_3O_4 are typical for nanometer-sized particles.

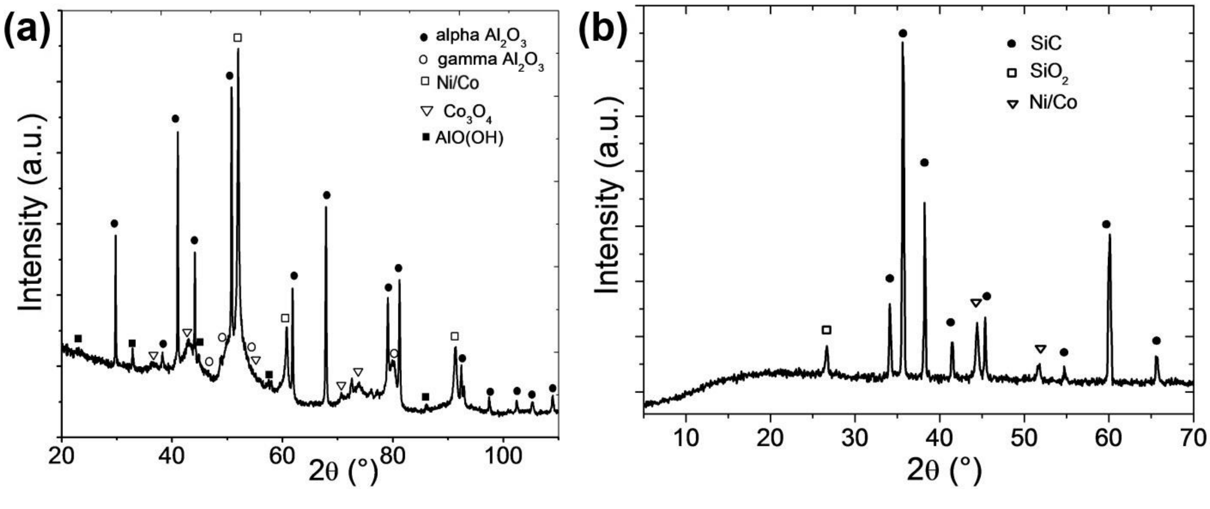

Figure 3. XRPD patterns of (a) 20 wt% $Co_{80}Ni_{20}/Al_2O_3$ and (b) 20 wt% $Co_{80}Ni_{20}$/SiC catalysts.

Narrow and very intensive reflexes of metals indicate large crystallite sizes. Metallic nickel and cobalt and their solid solutions have similar crystal structures. For this reason, it is almost impossible to separate the overlapping peaks for the observed diffraction pattern (Fig. 3a). High dispersion of the carrier can provoke the formation of amorphous cobalt metal at the stage of catalyst preparation. At the final stage of the catalyst preparation, the oxides of nickel and cobalt and their mixtures are reduced with hydrogen in the reactor immediately before the catalytic experiment. Therefore, one can assume that the catalyst surface during the course of CO_2 methanation is free of metal oxides. After a catalytic experiment, the reflexes of the Co_3O_4 phase, which appears, perhaps, because of surface passivation, were registered in the diffraction pattern of the 20 wt% $Co_{60}Ni_{40}/Al_2O_3$ catalyst. In the reaction medium, metallic nickel (in the micrometric particles) has lower oxygen reduction ability and oxidizes slower than metallic cobalt. That is why the reflexes related to the NiO phase are absent in the diffraction pattern.

For 20 wt% $Co_{80}Ni_{20}$/SiC catalysts, one can see crystalline phases of SiC, Ni/Co metal, and SiO_2, assuming the latter as the product of SiC oxidation (Figure 3b). Carborundum SiC has a geometric surface area, which value is much lower than that of the alumina, and, consequently, this carrier has an insignificant amount of functional surface groups. That is why microcrystals of metallic Ni and Co loaded on such an inert carrier are not subjected to deep oxidation when working in the reaction mixture.

CONCLUSIONS

From the results of the present study, we can draw the following conclusions about the behavior of methanation catalysts: the operating temperatures of 20 wt% Co–Ni/Al_2O_3 catalysts are much lower than those of the 20 wt% Co–Ni/SiC catalysts. The uniform distribution of the active Co–Ni metal mass on the surface of alumina increases the accessibility of active catalyst centers for the course of CO_2 methanation. An additional factor that, in our opinion, contributes to the methanation efficiency is the intensive microheterogeneity in the composition of the loaded Co–Ni active phase. Although the efficiency of 20 wt% $Co_{80}Ni_{20}$/SiC catalysts is lower than that of the 20 wt% $Co_{80}Ni_{20}/Al_2O_3$ catalysts, the latter provides better performance (100% conversion of CO_2 to CH_4) unlike the massive $Co_{80}Ni_{20}$ metallic catalyst giving the maximum methane yield of only 65% at above 450 °C [17]. For the Co-rich, high activity catalysts, the thermal desorption peaks for particles taking part in the CO_2 methanation reaction and adsorbed on the active sites are registered at the same temperature. The presence of CHO* formate intermediate registered for the studied catalysts confirms that the reaction takes place *via* intermediates under softer conditions and at a faster rate, which is the reason for the highest activity of the Co-rich bimetallic Co–Ni catalysts.

REFERENCES

1. W. Wang, S. Wang, X. Ma, J. Gong, *Chem. Soc. Rev.*, **40**, 3703 (2011).
2. T. A. LeJong, K. Kang, E. D. Park, *Top. Catal.*, **15-17**, 1537 (2018).
3. C. Liu, T. R. Cundari, A. K. Wilson, *J. Phys. Chem. C*, **116**, 5681 (2012).
4. M. Zhludenko, A. Dyachenko, O. Bieda, S. Gaidai, M. Filonenko, O. Ischenko, *Acta Phys. Polonica A*, **133**, 1084 (2018).
5. S. Hwang, J. Lee, U. G. Hong, J. H. Baik, D. J. Koh, H. Lim, I. K. Song, *Catal. Lett.*, **142**, 860 (2012).
6. S. Rahmani, M. Rezaei, F. Meshkani, *J. Ind. Eng. Chem.*, **20**, 1346 (2014).
7. M. J. Ledoux, C. Pham-Huu, *CATTECH*, **5**, 226 (2001).
8. M. Feyzi, A. Babakhanian, M. B. Gholivand, *Korean J. Chem. Eng.*, **31**, 37 (2014).
9. S. Carenco, C.-H. Wu, A. Shavorskiy, S. Alayoglu, G. A. Somorjai, H. Bluhm, *Small*, **11**, 3045 (2015).
10. D. Beierlein, D. Häussermann, M. Pfeifer, T. Schwarz, K. Stöwe, Y. Traa, E. Klemm, *Appl. Catal. B: Environ.*, **247**, 200 (2019).
11. R. Meshkini Far, O. V. Ishchenko, A. G. Dyachenko, O. Bieda, et al., *Funct. Mater. Lett.*, **11**, art. no. 1850057 (2018).
12. V. L. Veselovskyi, E. V. Ischenko, S. V. Gayday, V. V. Lisnyak, *Catal. Commun.*, **18**, 137 (2012).
13. A. Karelovic, P. Ruiz, *J. Catal.*, **301**, 141 (2013).
14. I. A. Fisher, A. T. Bell, *J. Catal.*, **162**, 54 (1996).
15. V. K. Yatsimirsky, V. L. Budarin, V. E. Diyuk, L.Y. Matzui, M. I. Zacharenko, *Adsorpt. Sci. Technol.*, **18**, 609 (2000).
16. A. V. Puga, *Catal. Sci. Technol.*, **8**, 5681 (2018).
17. O. V. Ishchenko, A. G. Dyachenko, A. V. Yatsymyrskiy, T. M. Zakharova, et al., *E_3S Web Conf.*, **154**, 02001 (2020).